Online Positioning of a Drone-Mounted Base Station in Emergency Scenarios

Pijnappel, T. R.; van den Berg, J. L.; Borst, S. C.; Litjens, R.

DOI
10.1109/TVT.2023.3329960

Publication date
2024

Document Version
Final published version

Published in
IEEE Transactions on Vehicular Technology

Online Positioning of a Drone-Mounted Base Station in Emergency Scenarios

T.R. Pijnappel, J.L. van den Berg, S.C. Borst, and R. Litjens

***Abstract*—Wireless communication networks provide a critical infrastructure, particularly in emergency situations due to disruptive events such as natural disasters or terrorist attacks. However, in these kinds of scenarios part of the network may no longer be operational and a traffic hotspot may emerge, which may result in coverage and/or capacity issues. Deploying self-steering drone-mounted base stations offers a potential method to quickly restore coverage and/or provide capacity relief in such situations, but appropriate positioning is crucial in order for a drone base station to be truly effective. Motivated by that challenge, we propose a data-driven algorithm to optimize the position of a drone base station in a scenario with a site failure and emergence of a traffic hotspot. We demonstrate that the use of a drone, when properly positioned, yields significant performance gains, and that our algorithm outperforms benchmark mechanisms in a wide range of scenarios. In addition, we show that our algorithm is able to find a near-optimal position for the drone in a reasonable amount of time, and even has the ability to track the optimal position in case of a moving hotspot.**

***Index Terms*—5G, drone base stations, drone base station positioning, data-driven algorithm, dynamic traffic hotspot.**

I. Introduction

THE key requirements in the planning and optimization of wireless cellular networks include the provisioning of adequate coverage and sufficient traffic handling capacity. While well-engineered networks meet these requirements in normal conditions, they may not be able to do so in situations where part of the network is no longer operational. Such situations may for example arise due to natural disasters such as earthquakes, floodings, or wildfires, or due to terrorist attacks. In these cases, it may be difficult, dangerous and/or time-consuming for a repair or maintenance team to access the affected area and restore the network operations. Especially in these kinds of situations the deployment of self-steering drone-mounted base stations offers a flexible and promising method to provide capacity relief and/or restore coverage. Also in case of events with massive crowds/traffic hotspots such as sports games, festivals or large-scale demonstrations, a network may face capacity issues and can therefore benefit from the deployment of drone base stations [1].

The effective deployment of a drone base station crucially relies on determining an appropriate 3D-position. A well-positioned drone can significantly improve performance as it is able to support users that otherwise would be unserved. Furthermore, served users may experience a stronger signal and experience less interference when served by the drone. On the other hand, a poorly positioned drone can potentially even degrade network performance as it may cause additional interference for users that are not connected to the drone. It can also be the case that the drone unintentionally attracts users that are better off when served by one of the still operational regular base stations and enjoying the benefits of e.g. their higher transmit power or enhanced beamforming capabilities.

The drone positioning problem is particularly challenging, since the optimal position depends on many aspects, including the nature of the scenario (crowded event or network disruption), and the generally unknown propagation characteristics and spatial user distribution. Moreover, in case of a network disruption involving both a site failure and the emergence of a traffic hotspot, optimizing the drone position may involve a challenging trade-off between bringing capacity to the traffic hotspot or alleviating a coverage hole induced by the site failure. This trade-off depends on the location and intensity of the hotspot, which are often not a priori known in practice. In this paper we develop an online control algorithm which addresses this trade-off and uses real-time and practically measurable data to find an appropriate position for a drone base station. For this we investigate the performance impact of different control parameters such as the drone's 3D-position and develop a drone positioning algorithm based on the most important control parameters.

The remainder of this paper is organized as follows. Section II-A provides a review of related literature and highlights the contribution of this work. In Section III the overall setting and the key performance metric that we consider throughout the paper are introduced. Section IV elaborates on the trade-offs and challenges in determining an appropriate position of a drone base station. In Section V we present the modeling assumptions underlying the conducted simulations, and subsequently discuss the results of a simulation-based sensitivity analysis involving a static drone in Section VI. The proposed data-driven drone positioning algorithm is specified in Section VII, followed by

Manuscript received 22 February 2023; revised 7 August 2023; accepted 11 September 2023. Date of publication 3 November 2023; date of current version 22 April 2024. This work was supported by the Netherlands Organisation for Scientific Research (NWO) through Gravitation-Grant under Grant NETWORKS-024.002.003. The review of this article was coordinated by Prof. Zhiguo Shi. *(Corresponding author: T.R. Pijnappel.)*

T.R. Pijnappel and S.C. Borst are with Eindhoven University of Technology, 5600 MB Eindhoven, The Netherlands (e-mail: t.r.pijnappel@tue.nl; s.c.borst@tue.nl).

J.L. van den Berg is with the University of Twente, 7522 NB Enschede, The Netherlands (e-mail: j.l.vandenberg@utwente.nl).

R. Litjens is with TNO, 2595 DA The Hague, The Netherlands, and also with Delft University of Technology, 2628 CD Delft, The Netherlands (e-mail: remco.litjens@tno.nl).

Digital Object Identifier 10.1109/TVT.2023.3329960

the results of a simulation study in Section VIII to examine the performance of the algorithm. Section IX summarizes the key conclusions and provides some topics for further research.

II. Related Literature and Contribution

This section provides an overview of related literature and highlights the contribution of this work.

A. Related Literature

Although drone base stations can be used in many situations [2], we focus our literature review on papers that consider their deployment for enhancing coverage and capacity in scenarios with crowded events and public safety settings. For this use case most papers aim to optimize the positioning of drones [3], [4], [5], [6], [7], [8], [9], [10], [11], [12], [13], [14], [15], [16], [17], [18], [19], [20], [21], [22] while some also optimize the number of drones that need to be deployed [3], [4], [5], [6].

In [3], the authors consider an entirely drone-based 3D cellular network providing wireless coverage to drone-based user equipments (UEs). To this end the authors approximate drone-specific coverage areas by truncated octahedron shapes to determine the required number of drone base stations and their positions.

In [4] a classical branch-and-bound algorithm with a relaxation-induced neighborhood search is compared with a low-complexity heuristic in the optimization of the number and location of drone base stations. The comparison shows that the heuristic tends to connect more users, but requires more drones to do so.

The study in [5] compares a simulated annealing approach and a genetic algorithm to minimize the number of drone base stations and optimize their 3D-positions for energy-efficient coverage provisioning. Another approach proposed by [6] and [7] is to use a particle swarm optimization algorithm to find suitable 3D-positions for drone cells. The proposed algorithm starts with a set of candidate solutions and tries to iteratively improve these solutions with respect to a given measure related to the capacity, coverage and spectral efficiency.

Software-defined networks offer a method that facilitates the execution of the algorithm and measurements, and is therefore suitable for the implementation of a drone positioning algorithm. E.g. [8] proposes a software-defined networking based approach to construct a more resilient network, where particle swarm optimization is used for the positioning of drones.

In [9] a 'sweep and search' procedure is proposed to find optimal locations for drone base stations with the goal to provide coverage to as many users as possible for a given constellation of users. To find the optimal positions for the drones, each drone is assigned a search area, where it searches for user clusters while following a zig-zag pattern.

In [10], [11], [12] the authors use Q-learning to find the optimal placement of drone base stations. [10] considers the use of a single drone base station in combination with existing regular base stations with the goal to maximize the aggregate network throughput. In [11] the use of multiple drone base stations is considered in a scenario without regular base stations. In this setting the authors aim to find optimal positions and transmit powers for the drones. [12] aims to maximize coverage in an emergency scenario by deploying a temporary network which consists of a truck base station and multiple drone base stations. A known drawback of the used Q-learning approach is that it requires a relatively long time to learn the environment, while in emergency scenarios it is of utmost importance that the system is quickly able to find the optimal positions and therefore does not require a long learning period.

The authors of [13] consider the optimization of the position of a drone base station in an online setting with user mobility. For this optimization the authors aim to minimize the path loss of the user with the highest path loss using a Q-learning approach, a gradient-based solution and a greedy algorithm.

In [14] a layered architecture is proposed where drones flying in swarms at different altitudes are considered as an integrated part of future cellular networks to provide additional capacity and expand coverage. In this work, the positioning of the drones at the lowest layer (the drones serving the users) is optimized using an exhaustive search, which is noted to be difficult in more complex scenarios.

Also the use of drones as relay stations is investigated by [15], [16], [17]. In [15] the authors aim to maximize throughput while taking into account the quality of service of the users, capacity of the backhaul, available bandwidth and available power. For this purpose the problem is decomposed into a 3D-positioning problem and a resource allocation problem which are solved using a cyclic iterative algorithm. Similarly, [16] designs a heuristic algorithm that jointly optimizes the placement of drone relays, user association and bandwidth allocation such that the number of served users in a disaster struck area is maximized. In [17] it is noted that both power allocation and positioning of the drones affect system performance. For this reason they develop criteria for optimal positioning and power allocation of the drone relays.

As drones carry a battery they can only be deployed for a limited amount of time. To overcome this issue, [18] proposes to provide power to the drone using a tether that connects the drone to the ground. For this setting, the authors study the optimal placement of such a drone within a so-called hovering region that depends on the tether length and surrounding buildings.

In [19] a sensitivity analysis regarding the position and cell selection bias is conducted. This analysis showed that in the given setting the CSR is not very sensitive to the position and cell selection bias when these are close to optimal.

In [20] the authors present an analytical approach to optimize the altitude of drone base stations to provide maximum radio coverage on the ground.

The authors of [21] propose to use a machine learning approach to detect overloaded cells and formulate an optimization problem for the deployment of drone base stations. This optimization problem aims to maximize the number of covered users in overloaded cells by finding the optimal 3D-placement of drones while minimizing the energy consumption of the drones.

As all reviewed papers consider different approaches, incorporate other system aspects and/or pursue different objectives, we highlight the novelty of our work in Table I where we indicate whether a few key aspects relating to the addressed scenario or

TABLE I
NOVEL ASPECTS OF CURRENT PAPER IN RELATION TO CLOSEST PRIOR WORK

	[4]	[6]	[7]	[9]	[10]	[11]	[12]	This paper
Mixed scenario with terrestrial and drone base stations	✗	✗	✓	✗	✓	✗	✓	✓
Use of operationally available measurement data	✓	✗	✓	✓	✓	✓	✓	✓
Scenario incorporates realistic dynamics in the user constellation	✗	✗	✗	✗	✗	✗	✗	✓

the pursued solution are covered by the most closely related references. Firstly, we indicate whether the studies consider mixed scenarios involving both terrestrial base stations and drone base stations or consider the use of drones only. Secondly, we specify whether the exploited measurements are or can be realistically made available in an operational setting, noting that a network is generally unaware of the fraction of users that have no coverage. In the final row we indicate whether the study optimizes drone positions (configurations) in a scenario with a realistic variation in the presence and/or location of users, or assumes a user constellation which remains constant throughout (parts of) the optimization process.

Although the solutions proposed by [4], [5], [6], [7], [8], [9], [10], [11], [12], [13], [14], [15], [16] seem reasonable, these solutions require the ability to evaluate the performance for all possible configurations of the drone locations at a given time. In order to do so, these papers effectively assume that the constellation of active users does not change while the algorithm searches for the optimal position. However, this assumption has practical limitations in dynamic settings as both the movement of a drone from one location to another as well as measuring the performance at a given location takes time, during which the constellation of active users is likely to change. To overcome this issue, the algorithm that we propose will naturally adapt to changes in the constellation of active users and can therefore be used in practice. Moreover, we will consider scenarios where a traffic hotspot moves around over time. Apart from the algorithm we proposed in [22] the aforementioned solutions from the literature are not designed for these kinds of scenarios.

B. Contributions

As mentioned earlier, it is challenging to find a good 3D-position for a drone base station as it depends on many aspects which are often unknown or difficult to measure. Therefore we propose and assess a data-driven algorithm that aims to find the optimal 3D-position in scenarios with a network disruption event (site failure) where a traffic hotspot may emerge. Compared to [22], we consider a broader range of scenarios (different hotspot locations for both urban and rural environments), as well as scenarios where the hotspot moves over time.

As opposed to [4], [5], [6], [7], [8], [9], [10], [11], [12], [13], [14], [15], [16] which optimize the drone position for snapshots of the environment (a given constellation of the user locations), we propose an algorithm that optimizes the drone location in an online manner. This means that the proposed algorithm naturally adapts to the changing environment. Furthermore, [4], [5], [6], [9], [11] only consider the use of drone base stations. In this paper we will also take still operational regular sites into account. For the described setting we initially consider four control parameters (the x, y, z coordinates and a cell selection bias known as the Cell Individual Offset or CIO), and show using a simulation-based sensitivity analysis that the altitude and CIO have limited impact on the chosen performance metric, the Call Success Rate (CSR).

Because of this observation, the proposed algorithm will only adjust the x and y coordinates of the drone. As it is not possible to accurately measure the CSR in short periods of time, we identify practically measurable metrics to drive the adjustments of the x and y coordinates. However, it is not clear what the most appropriate metric is to drive these adjustments. As the selection of such a metric is of great importance for our proposed method we investigate several metrics and compare their performance. The advantage of this approach is that it only relies on practically measurable metrics and does not require any pre-deployment learning or knowledge of the propagation environment, antenna features, location of the hotspot or traffic density. As a result, the proposed algorithm can be operationally deployed in a wide range of scenarios.

For the performance assessment of the algorithm we will examine a wide range of coverage and capacity-limited scenarios which correspond to both urban and rural environments. For these environments we consider various locations and traffic intensities of the hotspot. Moreover, we compare our algorithm with relevant benchmarks: i) no drone assistance; ii) a static drone deployed right above the failing site; iii) the algorithm proposed in [22]. We show that compared to these benchmarks our algorithm has a similar or improved performance in all scenarios. Lastly, we demonstrate that our algorithm is able to find a near-optimal position in a fairly short amount of time, and even is capable to track the optimal position in case of a moving traffic hotspot.

III. SCENARIOS AND PERFORMANCE METRIC

We consider a macro-cellular network whose service provisioning is impacted by a disruptive event, resulting in a site failure. As a consequence of this event, it may be the case that users are distressed which may lead to the emergence of a traffic hotspot. In this setting, we will consider a total of 44 scenarios, characterized by two distinct inter-site distances (ISDs) of 500 m and 3500 m (corresponding to an urban and a rural environment, respectively). For both the urban and rural environment we consider a case without a traffic hotspot and seven cases with distinct hotspot locations (marked by the cyan dots in Fig. 1). When a hotspot is present, we will consider three different relative traffic intensities in the hotspot. Hence the scenarios differ with respect to the type of environment (dense urban (DU) or rural (RU)), the location of the hotspot defined by the distance to the failing site d_{hotspot} (in m) and angle relative to the x-axis φ_{hotspot} (in degrees), and the relative traffic intensity in the hotspot ρ. In order to provide clear references to the various scenarios when presenting the numerical results, we

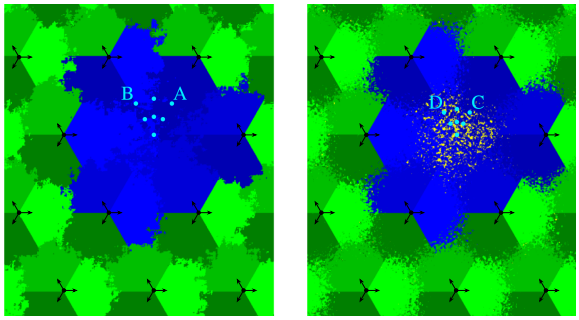

(a) (b)

Fig. 1. Best-server areas after the site failure. The different colored areas indicate the cells corresponding to the regular base stations. The yellow areas mark coverage holes. The black arrows show the azimuth directions of the still operational regular sites, and the cyan dots mark possible locations that we consider for the center of the hotspot. (a) Urban environment. (b) Rural environment.

denote them in the format "{DU, RU}-d_{hotspot}-φ_{hotspot}-ρ". For example "DU-100-90-4" refers to a scenario with a dense urban environment, a traffic hotspot located 100 m from the failing site at an angle of 90 degrees with respect to the x-axis where the traffic intensity is four times higher than elsewhere. While it is infeasible to exhaustively evaluate all possible scenarios (considering all possible hotspot locations and traffic intensities in the hotspot), the selected scenarios serve to cover a broad range of relevant environments and traffic patterns.

As mentioned earlier, we adopt the Call Success Rate (CSR) as performance metric to evaluate the performance in these scenarios. The CSR is defined as the fraction of calls that are successful, meaning that a call has coverage, is admitted to the system, is not dropped, and receives its required minimum bit rate for its entire duration. To determine the CSR we only consider calls that are initiated in the pre-incident best-server areas of the failing site and its immediate neighbor cells, indicated by the blue and yellow-shaded areas in Fig. 1, with the latter areas indicating coverage holes caused by the site failure.

IV. Key Challenges

In this section we will elaborate on various challenges and trade-offs associated with finding an appropriate position for a drone-mounted base station with respect to the CSR. To optimize the CSR, we consider four control parameters of the drone that can be adjusted, namely the x, y and z coordinates and the so-called Cell Individual Offset (CIO) which is used for cell selection (steering traffic towards or away from the drone) with the intention to better balance the loads of the drone and its neighboring cells.

A. 2D-Position Trade-off

One trade-off with respect to the 2D-position (x and y coordinates) of the drone arises when deciding whether to bring capacity to a hotspot area or to provide coverage near the failing site. If there is no hotspot, or the hotspot is not too intense, then it is likely best to position the drone right above the failing site. However, if there is a high traffic intensity in a hotspot area, then it may be better to position the drone close to this hotspot area to make sure that the users in the hotspot enjoy favorable radio conditions.

It is evident that the location of the hotspot is an important factor for the optimal drone position, but it is not only the distance between the hotspot and the failing site that matters. The position of the hotspot relative to the azimuth directions of the nearest still operational base stations is important as well, as it affects the degree to which those base stations can serve the hotspot traffic. Consequently, this also affects the degree to which the drone needs to move towards the hotspot and help out. To illustrate this, consider two scenarios: scenario A with a hotspot located such that the closest still operational regular site has an antenna aiming in the direction of the hotspot (indicated with the letter A in Fig. 1(a)), and scenario B with a hotspot located equally far from the failing site but with the nearest still operational regular cell aimed 60 degrees away from the hotspot (indicated with the letter B in Fig. 1(a)). For scenario A, the UEs in the hotspot have a relatively good connection to the regular base station compared to the hotspot UEs in scenario B. Therefore, in scenario A the drone can focus more on UEs close to the failing site, and hence the optimal position of the drone will be closer to the failing site.

B. Altitude Trade-off

The selection of the altitude involves a few trade-offs as well. First, a higher altitude implies that the distance between the drone and the UEs increases, which has a negative impact on the path loss, and therefore on the signal strength. Secondly, a higher altitude also has the advantage that there is a higher probability of having a line-of-sight (LoS) link with a UE, which in turn has a positive impact on the path loss and therefore on the signal strength. Lastly, an increased altitude has a positive impact on the antenna gain as the UEs will be closer to the antenna's main beam, which is directed downwards, which in turn has a positive impact on the signal strength. Overall, the net result of these counteracting effects is non-trivial and ultimately depends on the altitude of the drone and the 2D-distances between the UEs and the drone.

Because a change in altitude affects the signal strength, it also changes the area where the drone provides coverage. At the same time a change in altitude also affects the amount of resources that users require, which may lead to a trade-off between serving users with a good bit rate or providing coverage to a larger area.

C. CIO-Trade-off

As mentioned before, the CIO (given in dB throughout this paper) is used as a cell selection bias with the goal to balance the loads. For the cell selection, we look at all cells that provide coverage to the UE, and from these cells select the covering cell with the highest value of RSRP + CIO, where RSRP denotes the Reference Signal Received Power in dBm. Therefore the CIO is used to steer traffic towards (positive CIO) or away (negative CIO) from the drone to balance the loads between the drone and the other cells. So the difficulty in optimizing the CIO is finding a

CIO value which reduces the load of highly loaded cells without overloading the drone cell itself.

Moreover we should note that the altitude of the drone has a non-trivial impact on the optimal value of the CIO. The reason for this is that the altitude has an impact on the signal strength experienced by the UEs. If the UEs have a good signal, they require fewer resources and therefore the drone can support more UEs. However, as mentioned before, it is not clear how the altitude affects the signal strengths and therefore, it is unclear how the altitude affects the optimal CIO value.

V. Modeling Assumptions

In order to evaluate the performance of the proposed drone positioning algorithm, we will conduct extensive simulation experiments. In this section we give an overview of the modeling assumptions used in these simulations.

A. Network and Antenna Aspects

To model the network, we consider a hexagonal layout of twelve three-sectorized sites comprising $12 \times 3 = 36$ cells. We make a distinction between capacity-limited and coverage-limited scenarios, which we characterize by the assumption of an urban and a rural environment with inter-site distances (ISDs) of 500 m and 3500 m, respectively. We use a wraparound feature to mimic an infinite-size network and avoid boundary effects.

Each of these regular cells is assigned a $B = 5$ MHz carrier in the 3.5GHz band, where a fraction κ of the carrier is required for control signals. Furthermore, we assume that the drone is wirelessly backhauled on a frequency different from the frequency used to serve the UEs. Moreover, each regular cell is served by directional antennas located at an altitude of 25 m and 35 m for the urban and rural deployments, respectively[23, default values in Table 7.4.1-1]. For the antenna gains of the regular base stations we will use the model proposed in [24] characterized by the horizontal and vertical half-power beam widths $\text{HPBW}_{h,v}$ (in degrees), the maximum gain G_r (in dBi), the front back ratio FBR (in dB) and the side lobe level SLL (in dB). Given these, we can express the total antenna gain as $G(\varphi, \theta) = G_h(\varphi) + G_v(\theta)$ where

$$G_h(\varphi) = -\min\left\{12\left(\frac{\varphi}{\text{HPBW}_h}\right)^2, \text{FBR}_h\right\} + G_r, \quad (1)$$

$$G_v(\theta) = \max\left\{-12\left(\frac{\theta - \theta_{\text{etilt}}}{\text{HPBW}_v}\right)^2, \text{SLL}_v\right\}, \quad (2)$$

with φ denoting the horizontal angle relative to the azimuth direction, θ denoting the negative elevation angle relative to the horizontal plane and θ_{etilt} denoting the electrical downtilt. Furthermore we assume that all regular base stations have a total transmit power of $P_r^{\max} = 20$ W.

For the antenna gain of the drone base station we assume that the drone is equipped with an antenna consisting of a single antenna element. We then use a rotated version of the model provided in [23, Table 7.3-1], adapting the vertical component to ensure a circular footprint. As a result we model the antenna gain using the following formula

$$G(\varphi) = -\min\left\{12\left(\frac{\varphi}{\text{HPBW}_d}\right)^2, A_{\max}\right\} + G_d, \quad (3)$$

with $A_{\max}$ the maximum attenuation and G_d the maximum gain (both in dB). We assume that the drone has a total transmit power of $P_d^{\max} = 0.5$ W.

B. Propagation Characteristics

For the link between UEs and regular base stations we use the path loss models provided in [23, Tables 7.4.1 and 7.4.2]. We determine the path loss as the weighted average of the path loss for a line-of-sight (LoS) and a non-line-of-sight (NLoS) link, with weights given by the probability of having a LoS or NLoS link.

In view of the higher altitude and different orientation of the drone, we use a different path loss model for links between the UEs and the drone base station. For this model we need three statistical parameters to reflect different kinds of scattering environments [25]:

α: The ratio of built-up land area to the total land area.
β: The number of buildings per square kilometer.
γ: A scale parameter describing the buildings' heights according to a Rayleigh distribution.

Using these parameters we can determine two other environment parameters ξ and ψ according to [20]. Now we can formulate the path loss between the drone and a UE as the free space path loss plus an excessive path loss component η_{LoS} or η_{NLoS} which depends on the type of link (LoS or NLoS). In line with [20] the path loss is given by

$$L_d = 20\log_{10}\left(\frac{4\pi df}{c}\right) + p_{\text{LoS}}\eta_{\text{LoS}} + (1 - p_{\text{LoS}})\eta_{\text{NLoS}}, \quad (4)$$

where c denotes the speed of light, f the carrier frequency and d the 3D-distance between the drone and the UE, and

$$p_{\text{LoS}} = 1 - p_{\text{NLoS}} = \frac{1}{1 + \xi\exp\left(-\psi[\arctan(h/r) - \xi]\right)}, \quad (5)$$

with h and r the height difference and the horizontal distance between the UE and the drone, respectively.

Besides the path loss, the propagation loss of a signal is also affected by shadow fading. To incorporate this, we determine spatially and site-to-site correlated shadow fading maps for each of the sites according to the model provided in [26]. For this model we need to specify three parameters: the site-to-site correlation ω, the decorrelation distance d_{decorr} and the standard deviation of the shadow fading σ_{sh}.

Lastly, we impose a minimum coupling loss of 70 and 80 dB for the urban and rural environment, respectively [27].

C. Traffic Characteristics

We assume that the UEs that want to initiate a new call arrive according to a spatially uniform Poisson process with rate λ. In addition, we assume the emergence of a traffic hotspot that is caused by a network disruption event. This hotspot area is

assumed to be a circle with radius of 100 m, where the arrival rate of new calls is ρ times higher than elsewhere. The value of ρ and the location of the traffic hotspot will be varied in the different simulation scenarios.

All active UEs are assumed to be static (not moving over time) and the calls are assumed to have an exponentially distributed duration with a mean of τ seconds. Furthermore we assume that all calls require a minimum bit rate of R Mb/s for their entire duration.

D. Resource Management Aspects

Upon call generation, we first determine the RSRP values to the different cells to check whether the associated UE has coverage or not. When the UE has coverage, it is assigned to the covering cell with the highest value of RSRP + CIO. Then the admission control mechanism estimates the fraction of downlink resources that this new call requires such that it achieves its minimum required bit rate R. The required fraction of the serving cell's resources is estimated by $R/((1-\kappa)B\log_2(1+\text{SINR}))$, where SINR denotes the current Signal-to-Interference-plus-Noise Ratio experienced by the new UE, and B and κ are recalled to denote the available bandwidth and the fraction of this bandwidth required for control signals, respectively. For the calculation of the SINR, we assume a thermal noise of -106.94 dBm and a noise figure of 8 dB. The admission control mechanism admits the new call when sufficient resources can be made available without violating the minimum bit rate requirement of on-going calls.

In line with the aim to optimize the CSR, we assume a scheduling mechanism that allocates the available resources in a proportional fair way subject to the minimum bit rate requirement. In the unfortunate case where it is not possible to provide all assigned UEs with their required minimum bit rate (which can be a consequence of the drone movement as this impacts the signal strengths), as many UEs as possible receive the required amount of resources. In this case the remaining resources are given to the unsatisfied UE that requires the least amount of resources.

Although we do not consider user mobility, the dynamic adjustments of the drone position lead to changes in the path loss and antenna gain values. As a consequence, the total amount of required resources may exceed the available capacity, in which case at least one UE no longer receives its minimum required bit rate. Another consequence is that the RSRP values change as well and may result in the dropping of UEs. This happens when the RSRP of the serving cell falls below the coverage threshold of -120 dBm. Moreover, these changes in RSRP values can lead to handover requests when the RSRP + CIO of a candidate target cell exceeds the RSRP + CIO of the currently serving cell by at least 3 dB (assumed hysteresis value) for at least 200 ms (assumed time to trigger). When such a handover request is submitted to the target cell, the admission control treats this request in the same way as it treats a new UE. Whenever a handover request is denied, it is repeated after 50 ms provided that the conditions triggering the handover are still satisfied.

TABLE II
SIMULATION PARAMETERS

Parameter	Urban	Rural	Unit
ISD	500	3500	m
h_{UE}	1.5	1.5	m
α	0.5	0.05	
β	300	300	buildings/km^2
γ	20	4	
λ	1.3	0.018	arrivals/s/km^2
τ	120	120	s
κ	0.25	0.25	
R	0.4	0.4	Mb/s
G_r	15.4	15.4	dBi
HPBW$_h$	72	72	°
HPBW$_v$	5.6	5.6	°
FBR$_h$	24	24	dB
SLL$_v$	-11	-11	dB
θ_{etilt}	7	4	°
G_d	8	8	dBi
HPBW$_d$	65	65	°
$A_{\max}$	30	30	dB
η_{LoS}	1.7	0.1	dB
η_{NLoS}	24	22	dB
d_{decorr}	45	80	m
σ_{sh}	5	6	dB
ω	0.5	0.5	

E. Simulation Parameters

To be able to use the described models, we need to select suitable parameter values for our simulations. The selection is based on the ones indicated in a 3GPP technical report [23], a commonly known reference [29], and an antenna data sheet [30]. An overview of the selected parameters for both types of environments is shown in Table II.

VI. Sensitivity Analysis

In Section IV we gave some intuition for the optimal values of the control variables (x, y, z and CIO). Since it is not clear how and to what extent these control parameters affect the CSR performance, we conducted a simulation-based sensitivity analysis involving a static drone. In this sensitivity analysis we consider each of the 44 scenarios introduced in Section III. For each scenario we consider 21 different drone positions in the horizontal plane (specified relative to the locations of the hotspot and failing site), altitudes in $\{80, 90, \ldots, 200\}$ m and CIO values in $\{-4, -3, \ldots, 3, 4\}$ dB for the drone. For each combination of these parameters we determine the CSR averaged over twenty simulation runs with distinct random seeds, each covering a time span of one hour.

A. 2D-Position

As mentioned in Section IV-A, the location and intensity of the hotspot impact the optimal settings of the control parameters. To illustrate the impact of the hotspot intensity, consider an urban environment where the center of the hotspot is indicated with the letter A in Fig. 1(a). Fig. 2(a) and (b) show the results of a

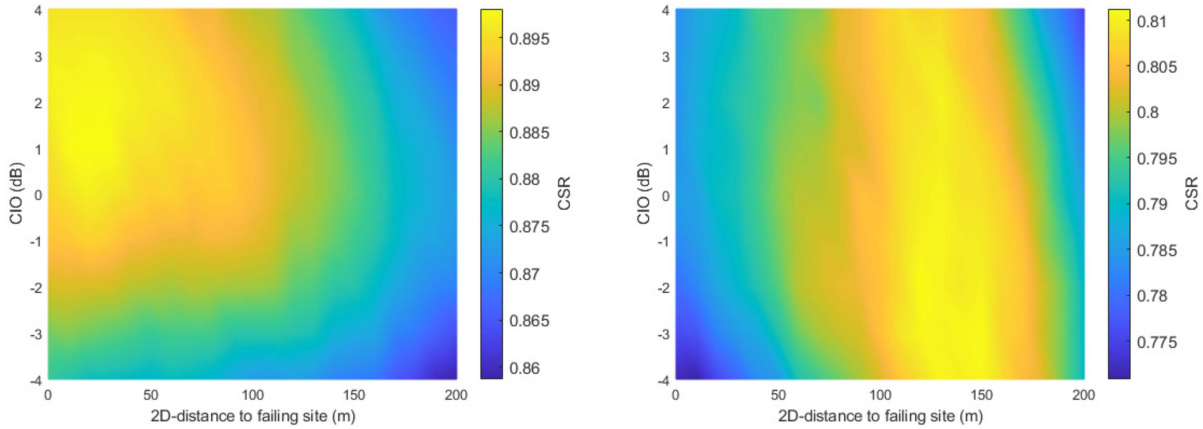

(a) (b)

Fig. 2. CSR for low (a) and high (b) traffic intensities in the hotspot, for various combinations of CIO values and positions of the drone on the line between the failing site and the center of the hotspot. (a) Low traffic intensity in the hotspot. (b) High traffic intensity in the hotspot.

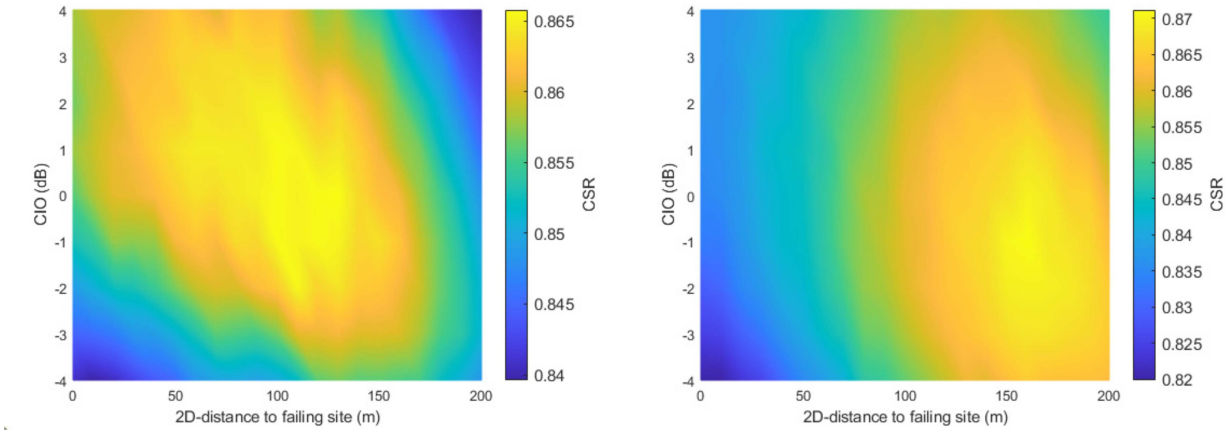

(a) (b)

Fig. 3. CSR for two different hotspot locations (A and B) with equal traffic intensity, for various combinations of CIO values and positions of the drone on the line between the failing site and the center of the hotspot. (a) Scenario A, hotspot located in the azimuth direction of a nearby cell. (b) Scenario B, hotspot located at 60 degrees from the azimuth direction of a nearby cell.

sensitivity analysis assessing the impact of the drone position and the CIO on the CSR for a scenario with a low and a high traffic intensity in the hotspot, respectively. In these figures, the positions of the drone are along the line from the failing site (2D-distance 0 m) to the center of the hotspot (2D-distance 200 m) for a fixed altitude of 120 m. The figures indeed show that the optimal position (with respect to the CSR) of the drone is close to the failing site for a low-intensity hotspot, while it is close to the center of the hotspot when the traffic intensity in the hotspot is high. Moreover, we see that the optimal value of the CIO is different for the two scenarios, which we will further discuss in Section IV-C.

In Section IV-A we also mentioned that optimal settings of the control parameters depends on the location of the hotspot relative to the azimuth directions of the nearest still operational base stations. To qualitatively illustrate this, we plot in Fig. 3(a) and (b) the CSR for different locations of the drone for scenarios A and B (as defined in Section IV-A), respectively. Again, we vary the CIO value and fix the altitude of the drone at 120 m. In line with the argumentation provided in Section IV-A, the figures show that the optimal position of the drone is closer to the failing site in scenario A than in scenario B.

B. Altitude

Let us first consider the RSRP values for UEs located at various distances from the drone for different altitudes of the drone as plotted in Fig. 4. In this figure the colors indicate the signal strength, and the white colored area indicates UE locations without coverage. We see that the coverage area increases with the altitude. Apparently, for most UE locations the positive effects of increasing the altitude on the antenna gain and LoS probability for the path loss outweigh the negative impact on the path loss caused by the increased distance between the UE and the drone. However, we note that in practice some legal restrictions may be in place for the altitude at which a drone

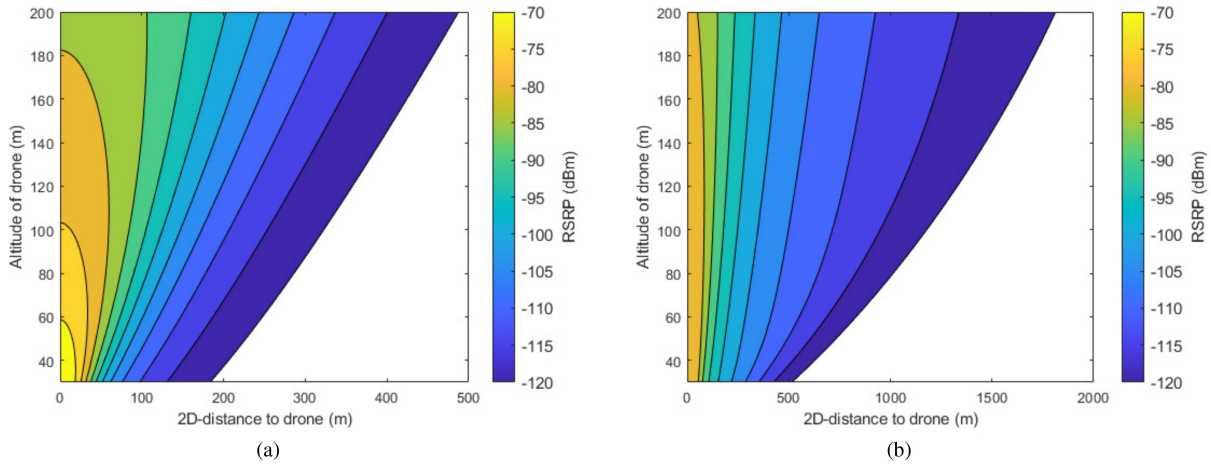

Fig. 4. RSRP values for various altitudes and 2D-distances in an urban (a) and rural (b) environment, respectively. (a) Urban environment. (b) Rural environment.

is allowed to fly. In this study we will restrict the drone to fly at an altitude up to 120 m which is the maximum allowed altitude for drones in the 'open' category [28], meaning that no special permit is required. However, it might be possible to avoid this restriction and potentially achieve better performance when considering drones in the 'specific' or 'certified' category.

As we can see in Fig. 4, increasing the altitude of the drone deteriorates the RSRP for UEs close to the main beam of the drone (2D-distance 0 m). This is caused by the fact that the path loss deteriorates more than the antenna gain improves. On the other hand, we also see that for UEs further away from the drone an increased drone altitude enhances the RSRP, as for these UEs the positive effects of the increased altitude on the path loss (due to an increased LoS probability) and antenna gain outweigh the negative effect of the increased distance on the path loss. Although from a coverage perspective it is best to position the drone at an altitude of 120 m given the assumed legal restriction, it is not clear whether this is also a good choice from a CSR point of view, where we should keep in mind that the still operational regular base stations also provide coverage to the area previously covered by the failing site. However, in 37 out of 44 scenarios in our simulation study, we observed that the optimal altitude from a CSR viewpoint was 120 m or higher. In Section VI-D we will further investigate the impact of the altitude on the CSR.

C. Cell Individual Offset

To illustrate the impact of the CIO we consider two scenarios where the hotspot is located at the same position (200 m from the failing site), but has a different traffic intensity ($\rho = 2$ and $\rho = 8$). In Fig. 2(a) and (b) we plot the CSR for various locations of the drone on the line from the failing site to the center of the hotspot but at a fixed altitude of 120 m, and for various values of the CIO. In these figures we observe that the CIO value optimizing the CSR is lower when the traffic intensity in the hotspot is higher. A reason for this is that when the traffic intensity increases, the drone will at some point no longer be able to support all UEs in its close proximity, and thus needs to steer some of this traffic towards regular cells that still can support these UEs. This illustrates that the CIO has a non-trivial impact on blocking and hence also on the CSR. However, in our simulation study we found that in 38 out of 44 scenarios the CIO optimizing the CSR lies in the interval from -2 to 2 dB. Moreover, the scenarios where this is not the case correspond to an ISD of 500 m (urban environment) and an eight times higher traffic intensity in the hotspot than elsewhere. We also see however that the CSR seems not too sensitive with respect to the CIO, therefore it appears to be possible to fix the CIO and still attain a close-to-optimal CSR.

D. Selection of the Altitude and CIO

As mentioned in Sections VI-B and VI-C, the optimal altitude and CIO were in most cases 120 m or higher and between -2 and 2 dB, respectively. Motivated by this observation, we investigate whether the sacrifice in terms of a reduced CSR is acceptable in case we choose to simplify the optimization challenge by fixing the altitude to 120 m and the CIO to 0 dB. The corresponding simulation results, shown in Fig. 5, reveal that the pairwise difference between the CSR values is small, with an average difference of approximately 0.004 and a maximum difference less than 0.012. Based on this insight, we choose to fix the altitude and the CIO to the given settings in the remainder of this paper, and concentrate on the dynamic optimization of the drone's 2D-position.

VII. Algorithms

In this section we specify the proposed data-driven drone positioning algorithm. For this we will elaborate on the algorithmic challenges, and describe the general framework of the proposed data-driven drone positioning algorithm and used control metrics (measurement data).

A. Algorithmic Challenges

Although we reduce the complexity from four optimization variables to only two by fixing the altitude and the CIO (as

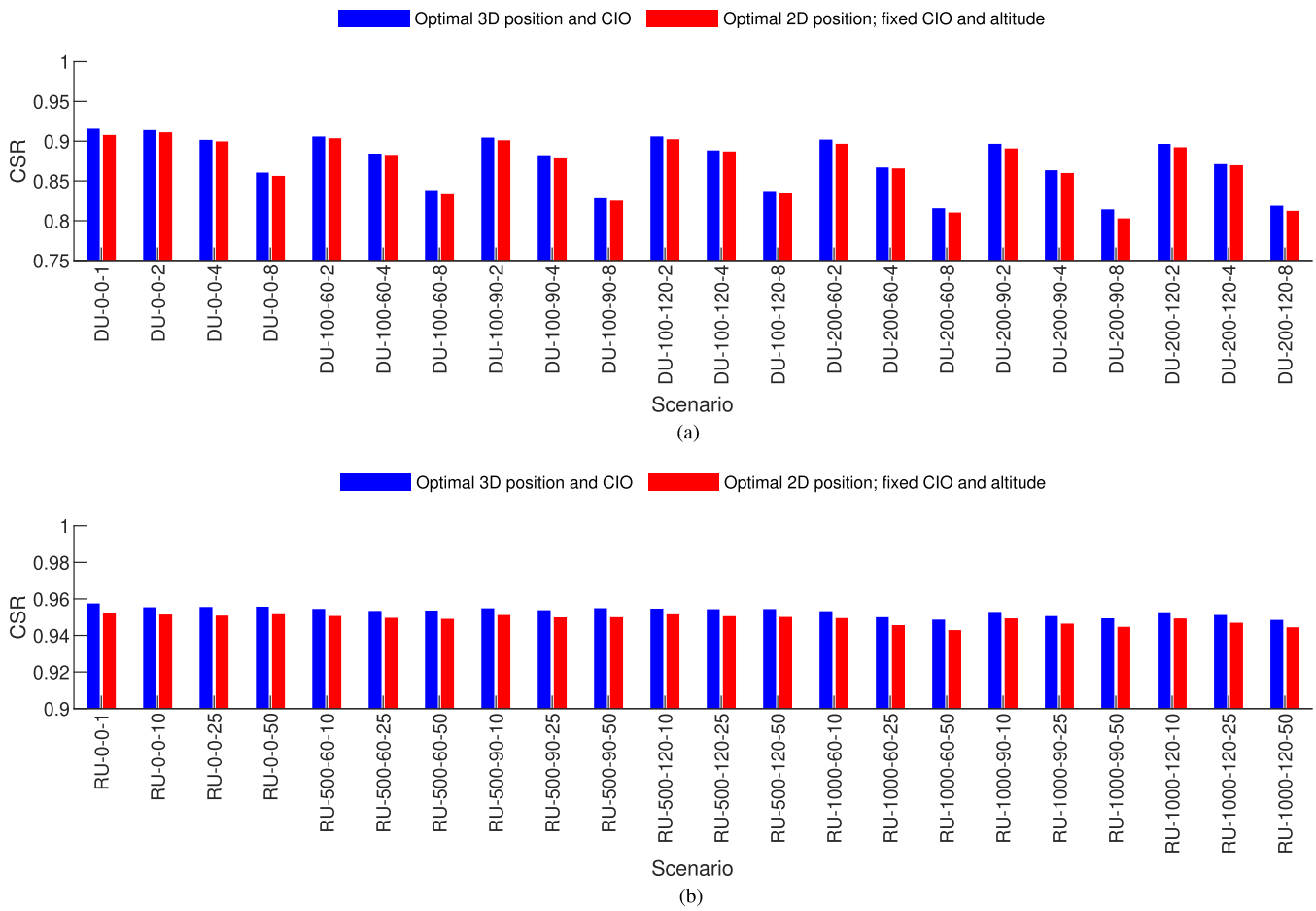

Fig. 5. Comparison of optimal CSR values for different scenarios, when the altitude and CIO are optimized, or fixed at 120 m and 0 dB, respectively. (a) Urban environment. (b) Rural environment.

mentioned in Section VI-D), finding the optimal horizontal drone position still constitutes a significant challenge. Moreover, because the optimal position of the drone depends on many unknown factors like the location and intensity of the hotspot, we need an online algorithm that can find an effective position for the drone with close-to-optimal CSR, in a fairly short amount of time (order of minutes).

Since we use the CSR as the main performance measure, it seems natural to use this metric also to drive the adjustments of the drone position. However, the CSR cannot be measured accurately in short periods of time for several reasons. First of all, the drone and other cells are unaware of UEs that do not have coverage. Secondly, a large number of calls needs to be considered to have an accurate measurement of the CSR. Hence, the CSR is ill-suited to drive the online adjustments of the drone position. Thus, we need another so-called control metric (CM) to drive the algorithm, whose optimization ideally leads to the same drone location that optimizes the CSR itself. Therefore the main novel component of the algorithm that we propose is the construction of this CM, which should be accurately measurable in relatively short amounts of time. In Section VII-C we will propose several choices for the CM which will be evaluated in Section VIII-A, where each CM is used in combination with the general algorithmic framework presented in the next section.

B. General Framework

We consider a measurement-based algorithm that adjusts the location of the drone (x and y coordinates) in an iterative manner, where only one coordinate is adjusted at a time. For these adjustments we start by measuring a CM that can be measured accurately in a relatively short amount of time (which we assume to be 200 ms). The measurement is followed by a 'decision point', at which the algorithm takes the action to move one meter in the x or y direction with an assumed speed of 24 km/h. When the drone has moved to the new position, we wait some time, the so-called 'time to trigger' which is assumed to be 200 ms to allow handovers to occur as a possible consequence of the action. After that a new measurement period starts followed by a new decision point. At this decision point the algorithm needs to select the next action based on the previous actions and the current and previous CM. If the CM has improved, then it is assumed that the previous action was a good one and the same action is repeated until the CM starts to degrade. In case the CM degraded, the previous action is assumed to be a bad one, and the algorithm starts adjusting the given coordinate (x or y) in the opposite direction until the CM degrades again. At that point, we start optimizing the other coordinate. An overview of the algorithm is shown in Fig. 6. Although the 'flowchart logic' of the algorithm itself

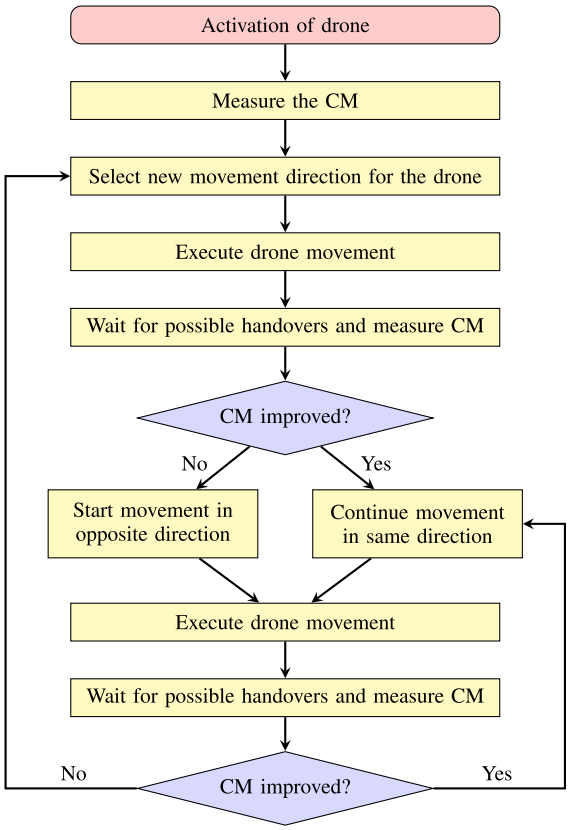

Fig. 6. Flowchart of the algorithm.

is fairly straightforward, the innovative aspect of the algorithm lies in the use of a carefully defined CM to drive the adjustments of the drone with the goal to optimize the CSR. Note that it is unclear what CM would best achieve this goal as the CSR cannot be used to drive the drone adjustments. Furthermore, as the constellation of calls changes over time, the optimal position of the drone changes over time as well. Hence, an action that is considered good at time t may be considered bad at time $t + \Delta t$, which implies that the drone needs to continuously optimize its position based on the CM.

We would like to emphasize that the described algorithm only relies on practically measurable metrics and does not require any pre-deployment learning or knowledge of the propagation environment, antenna features, location of the hotspot or traffic density. As a result, the algorithm can be used in a wide range of scenarios.

C. Control Metrics

As mentioned, the CM is at the core of the algorithm and has a significant impact on the performance of the algorithm and thus the CSR. Hence, it is important to select a suitable CM, which can be easily obtained in practice. An example of a metric that is easy to measure in practice relates to the load of a cell, which we define to be the fraction of resources that a cell needs to provide all its assigned UEs their minimum required bit rate. These load measurements indirectly provide an indication for the degree of blocking and thus the CSR, and therefore form a natural basis for the CMs. The idea behind this is that minimizing the cell load or, alternatively, the load per UE leads to more available resources, hence a reduction of the number of blocked UEs and therefore an improvement of the CSR.

A key question is for which cell we consider the cell load or load per UE. An obvious choice seems to be to consider the drone cell, but it could also be beneficial to reduce the load (per UE) in the most highly loaded regular cell adjacent to the cells of the failing site. Based on this, we choose to consider the following CMs:

CM 1: The load of the drone cell.
CM 2: The load of the most highly loaded regular cell.
CM 3: The load of the drone cell plus the load of the most highly loaded regular cell.
CM 4: The average load per UE of the drone cell.
CM 5: The average load per UE of the most highly loaded regular cell.
CM 6: The average load per UE of the drone cell and the most highly loaded regular cell (each cell has equal weight).
CM 7: The average load per UE of the drone cell and the most highly loaded regular cell (each cell has weight equal to the number of assigned UEs).

In the description above, a regular cell is considered to be one of the cells adjacent to the cells of the failing site. In an operational network, the values of these CMs are readily collected by a control node, which can then determine the next action and signal this to the drone.

VIII. Simulation Results

Using the models described in Section V, we evaluate the performance of our algorithm with the CMs described in Section VII. In particular, the resulting CSR values will be considered for the 44 scenarios with a static hotspot as described in Section III. Moreover, we consider the convergence time of the proposed algorithm using the best performing CM, and evaluate the tracking capabilities of the drone in case of a moving hotspot.

A. Static Hotspots

Let us first consider the performance of the proposed algorithm with each of the chosen CMs, for the scenarios with static hotspots described in Section III. Besides the scenario without a hotspot, we assume the multiplication factor for the intensity of initiated calls in the hotspot ρ to be 2, 4 or 8 for the urban environment, and 10, 25 and 50 for the rural environment. In all scenarios, the starting position of the drone is above the failing site and that the location of the center of the hotspot is static (does not change). To get accurate results, we determine the average CSR over 25 simulation runs where for each run the CSR is measured over a time period of four hours starting when the drone has been active for some time.

Table III shows the performance of the three benchmarks (no drone, a static drone above the failing site and the algorithm from [22]) and the proposed algorithm using the different CMs as listed in Section VII-C. As expected, the setting without a drone has the worst CSR performance for most scenarios. However,

TABLE III
CSR OF THE BENCHMARKS AND PROPOSED ALGORITHM WITH DIFFERENT CMS

Scenario	No drone	Static	Algo [22]	CM 1	CM 2	CM 3	CM 4	CM 5	CM 6	CM 7
DU-0-0-1	0.849	0.908	0.904	0.902	0.850	0.905	0.902	0.849	0.904	0.906
DU-0-0-2	0.817	0.908	0.905	0.905	0.816	0.908	0.905	0.816	0.908	0.908
DU-0-0-4	0.760	0.901	0.895	0.900	0.760	0.903	0.900	0.760	0.903	0.903
DU-0-0-8	0.667	0.857	0.836	0.857	0.744	0.858	0.857	0.673	0.857	0.859
DU-100-60-2	0.822	0.899	0.897	0.897	0.823	0.901	0.896	0.823	0.899	0.899
DU-100-60-4	0.773	0.875	0.877	0.883	0.773	0.885	0.883	0.774	0.886	0.886
DU-100-60-8	0.688	0.814	0.820	0.827	0.701	0.828	0.827	0.689	0.827	0.827
DU-100-90-2	0.820	0.897	0.895	0.894	0.820	0.898	0.895	0.821	0.898	0.898
DU-100-90-4	0.768	0.870	0.872	0.882	0.768	0.884	0.881	0.769	0.883	0.884
DU-100-90-8	0.682	0.808	0.811	0.826	0.684	0.826	0.825	0.682	0.825	0.827
DU-100-120-2	0.819	0.895	0.897	0.897	0.819	0.900	0.897	0.819	0.899	0.899
DU-100-120-4	0.765	0.865	0.881	0.888	0.766	0.890	0.888	0.766	0.890	0.890
DU-100-120-8	0.674	0.801	0.820	0.836	0.677	0.837	0.836	0.676	0.835	0.836
DU-200-60-2	0.832	0.893	0.889	0.887	0.833	0.891	0.888	0.833	0.890	0.891
DU-200-60-4	0.798	0.858	0.857	0.860	0.797	0.864	0.860	0.798	0.862	0.863
DU-200-60-8	0.723	0.783	0.789	0.790	0.722	0.794	0.790	0.724	0.794	0.794
DU-200-90-2	0.828	0.888	0.883	0.883	0.830	0.886	0.883	0.829	0.887	0.886
DU-200-90-4	0.787	0.846	0.857	0.863	0.787	0.865	0.862	0.787	0.865	0.865
DU-200-90-8	0.707	0.767	0.787	0.796	0.709	0.798	0.796	0.709	0.797	0.798
DU-200-120-2	0.825	0.885	0.885	0.884	0.826	0.888	0.885	0.826	0.887	0.888
DU-200-120-4	0.778	0.836	0.862	0.867	0.779	0.868	0.867	0.779	0.869	0.868
DU-200-120-8	0.692	0.747	0.795	0.800	0.695	0.802	0.800	0.695	0.802	0.803
RU-0-0-1	0.906	0.951	0.947	0.948	0.908	0.949	0.948	0.908	0.949	0.950
RU-0-0-10	0.900	0.951	0.949	0.950	0.902	0.950	0.950	0.902	0.951	0.951
RU-0-0-25	0.891	0.952	0.949	0.951	0.895	0.952	0.951	0.895	0.952	0.952
RU-0-0-50	0.874	0.951	0.949	0.952	0.882	0.952	0.951	0.884	0.952	0.952
RU-500-60-10	0.902	0.950	0.947	0.948	0.904	0.949	0.948	0.905	0.949	0.950
RU-500-60-25	0.896	0.949	0.948	0.949	0.900	0.950	0.949	0.898	0.950	0.950
RU-500-60-50	0.882	0.944	0.946	0.949	0.888	0.949	0.948	0.890	0.949	0.949
RU-500-90-10	0.901	0.951	0.948	0.948	0.903	0.949	0.949	0.903	0.949	0.950
RU-500-90-25	0.893	0.950	0.947	0.949	0.898	0.950	0.949	0.896	0.950	0.950
RU-500-90-50	0.878	0.946	0.947	0.949	0.885	0.949	0.949	0.885	0.949	0.949
RU-500-120-10	0.900	0.951	0.947	0.949	0.903	0.949	0.949	0.903	0.949	0.949
RU-500-120-25	0.893	0.950	0.948	0.949	0.897	0.950	0.949	0.896	0.950	0.950
RU-500-120-50	0.878	0.946	0.947	0.948	0.884	0.949	0.949	0.885	0.949	0.949
RU-1000-60-10	0.903	0.949	0.945	0.947	0.905	0.947	0.947	0.905	0.947	0.947
RU-1000-60-25	0.899	0.944	0.942	0.944	0.900	0.945	0.944	0.900	0.945	0.944
RU-1000-60-50	0.889	0.934	0.939	0.942	0.890	0.941	0.942	0.890	0.942	0.941
RU-1000-90-10	0.902	0.949	0.945	0.946	0.904	0.947	0.947	0.904	0.948	0.948
RU-1000-90-25	0.896	0.944	0.944	0.946	0.898	0.946	0.945	0.898	0.946	0.946
RU-1000-90-50	0.882	0.933	0.941	0.943	0.887	0.944	0.943	0.886	0.944	0.944
RU-1000-120-10	0.900	0.948	0.945	0.946	0.903	0.947	0.946	0.903	0.947	0.947
RU-1000-120-25	0.893	0.943	0.943	0.944	0.896	0.945	0.944	0.896	0.945	0.945
RU-1000-120-50	0.877	0.931	0.942	0.943	0.881	0.943	0.943	0.883	0.944	0.943

CM 2 and 5 have a poor performance, which is caused by the fact that the drone tends to move in the wrong direction. To explain this, notice that only the load or load per UE of the most highly loaded regular cell is considered. Moving the drone towards this cell implies additional interference for the UEs connected to this regular cell, which then need a larger fraction of the available resources. Hence the CM (load or load per UE) in this cell increases while we are trying to minimize the CM, meaning that it is better for the drone to move away from this cell.

We see that the static drone above the failing site performs quite well in a number of scenarios. The scenarios where this is the case have in common that there is no hotspot or a hotspot with a relatively low intensity of initiated calls ($\rho = 2$ in the urban setting and $\rho = 10$ in the rural setting), but also when the center of the hotspot is relatively close to the failing site.

Although the algorithm in [22] can make adjustments with respect to the altitude (but also has a maximum altitude of 120 m) and CIO, the proposed algorithm shows similar performance with CM 1 and 4. However, the proposed algorithm has in most scenarios a higher CSR with CM 3, 6 and 7 which is thanks to the fact that these consider both the drone cell and the most highly loaded regular cell. As it depends on the scenario which of the three CMs performs best, we will select the CM with the best CSR over all scenarios, which turns out to be CM 7.

As mentioned earlier, the performance improvement that can be realized by the deployment of a drone base station depends on the scenario. The proposed algorithm using CM 7 has at least a similar performance to the deployment of a drone above the failing site, but in some scenarios the proposed algorithm provides a significant performance improvement over such a static deployment. Examples of these scenarios are scenarios DU-100-120-4, DU-100-120-8, DU-200-90-4, DU-200-90-8, DU-200-120-4 and DU-200-120-8. In these cases we see improvements in CSR of more than 0.025, 0.035, 0.018, 0.030, 0.031 and 0.055, respectively. Although these values may seem to indicate rather modest improvements, they imply a reduction in the fraction of failed calls with more than 18%, 17%, 11%, 12%, 18% and 21%, respectively. This means for example for scenario DU-200-120-8 that more than one out of five calls that would be unsuccessful when deploying a static drone at the failing site would be successful when the drone would adjust its position using the proposed algorithm. Hence in several scenarios, the algorithm is able to dynamically find a better position for the drone which significantly reduces the fraction of failed calls.

In Fig. 7 we compare the proposed algorithm using CM 7 with the three benchmark settings (no drone, a static drone above the failing site and a drone that adjusts its x, y, z and CIO using the algorithm proposed in [22]). For these settings the average width of the two-sided 95% confidence intervals is less than 0.004, i.e. around 0.45% of the indicated value. Hence we see that the proposed algorithm significantly outperforms all benchmarks in scenarios considering a dense urban environment where the hotspot is not located at the failing site and has a load that is four or eight times higher than elsewhere. For all other scenarios, the proposed algorithm and the best-performing benchmark have overlapping confidence intervals, which indicates that in these scenarios the proposed algorithm has a performance similar to the best-performing benchmark.

B. Convergence Time

In an emergency scenario it is of utmost importance that the drone is able to find a good position in a fairly short amount of time. In order to investigate the convergence time (the time that the drone needs to find a good position), we plot the average CSR of 25 simulation runs measured over a moving time window of 5 minutes over time. For the urban environment we will consider the scenarios where the hotspot is located at positions A and B in Fig. 1(a), as well as a hotspot with its center at the failed site.

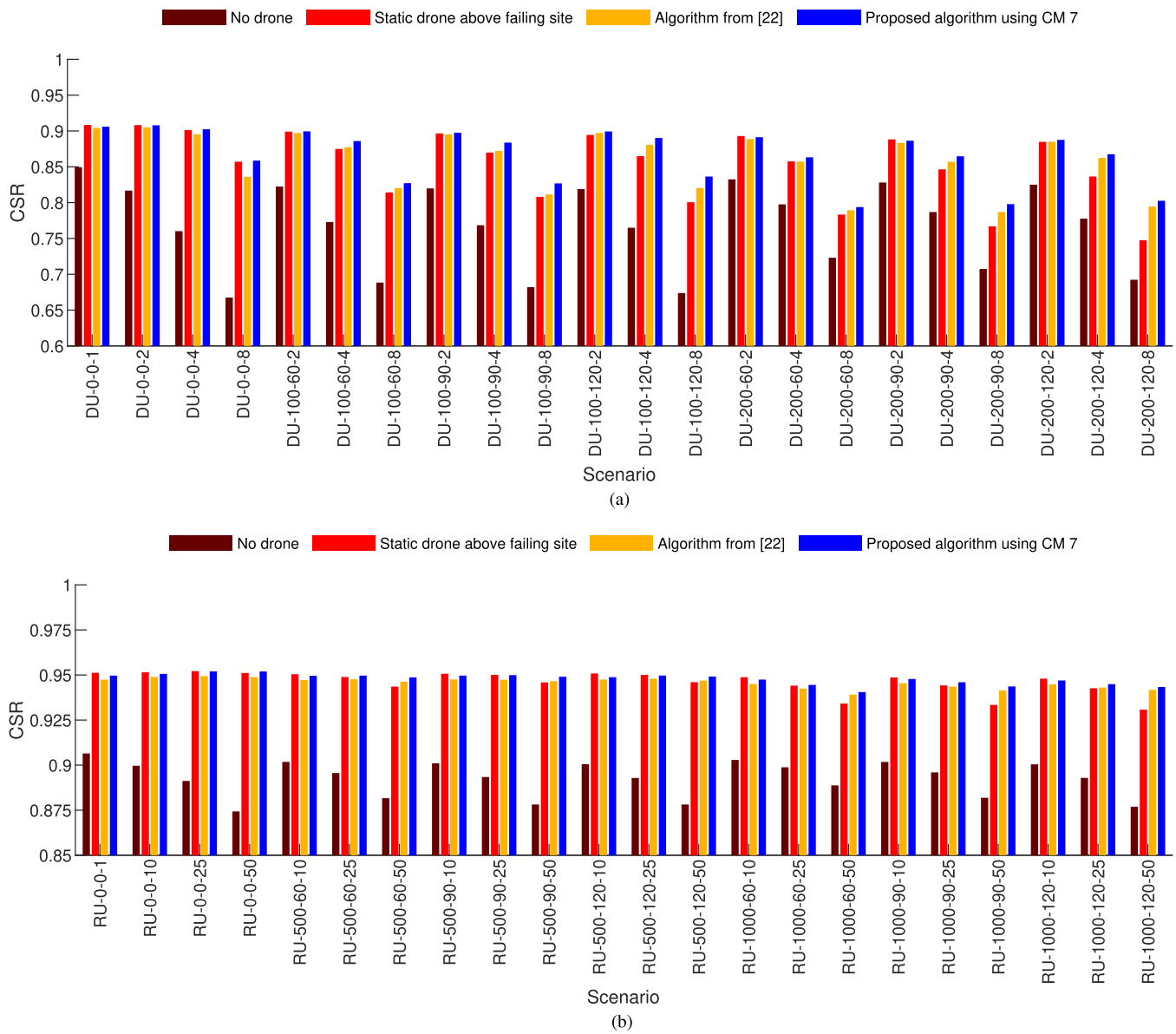

Fig. 7. Comparison of CSR corresponding to the proposed algorithm using CM 7 with the three benchmarks. (a) Urban environment. (b) Rural environment.

For these hotspot locations we will consider the traffic intensity in the hotspot to be twice or eight times as high as elsewhere i.e. $\rho \in \{2, 8\}$. Similarly, in the rural setting we will consider the locations C and D in Fig. 1(b) as well as the location of the failing site as the center of the hotspot, but now we will consider the traffic intensity in the hotspot to be 10 or 50 times as high as elsewhere i.e. $\rho \in \{10, 50\}$.

Before we discuss Fig. 8, we notice that the CSR value at time t is measured over the time window from time $t - 300$ to t. Furthermore, time 0 indicates the point in time where the drone becomes active. Therefore, it is logical that the CSR increases shortly after this, as the drone is then able to admit all new users and is gradually using more of its capacity.

For the scenario with the hotspot at the failing site and for the scenarios with the hotspot at locations A and B with $\rho = 2$, Fig. 8(a) shows that the CSR is fluctuating around an equilibrium after only 5 minutes. This can be explained by the fact that in these scenarios a good position for the drone is close to the failing site (where the drone starts at time 0). However, for the scenarios where the hotspot is located at location A or B with $\rho = 8$, we see that it takes approximately 1400 seconds to reach an equilibrium. Furthermore, we see in Fig. 8(a) that the settings with $\rho = 8$ have lower CSR compared to the settings with $\rho = 2$. To explain this, we note that the urban environment with an ISD of 500 m corresponds to a capacity-limited scenario. Hence for higher values of ρ, there is more traffic that cannot be served, resulting in a lower CSR.

When we consider the rural environment, Fig. 8(b) shows that for all scenarios the CSR fluctuates around an equilibrium value after 5 minutes. The explanation for this is that the rural environment corresponds to a coverage-limited setting. This means that a failing site results in areas without coverage, but also that UEs in areas around these coverage holes have a bad signal strength, and thus when admitted require large amounts

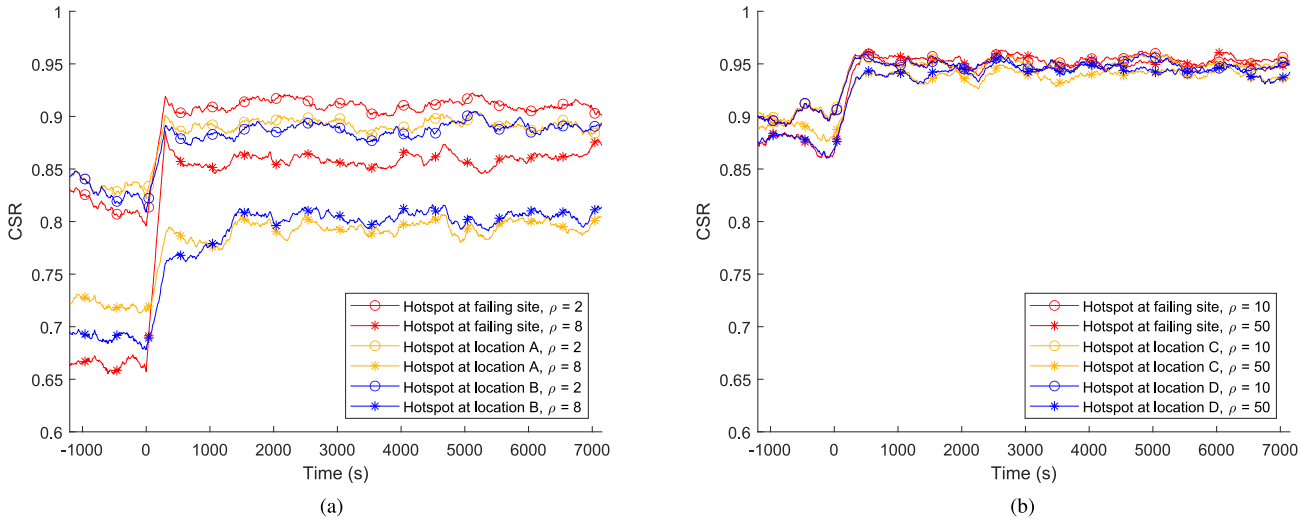

Fig. 8. CSR over time measured over 5-minute time windows. (a) Urban environment. (b) Rural environment.

of the available resources. As we see in Fig. 1(b), these areas without coverage, and thus also areas where UEs need a large fraction of resources, are more prominent close to the failing site. Therefore, a drone positioned above the failing site already improves the CSR significantly, and turns out to leave little room for further improvements.

Although the presented results are for CM 7, the other CMs except 2 and 5 (which had bad performance as indicated in Table III) show similar behavior.

C. Moving Hotspots

So far we have only considered static hotspots. However in an emergency situation hotspots may move, for example when a crowd tries to get away from the impacted area. In these kinds of situations, it is important for our algorithm to keep adjusting the drone position to serve as many UEs as possible. As we have seen in Section VIII-B, the position of the drone is most important in the urban setting, when there is a high traffic intensity in the hotspot. Therefore, we will focus on the urban environment, where we have a hotspot moving i) counterclockwise in a circle around the failing site, ii) back and forth in a straight line through the failing site at two different angles relative to the azimuth directions of the failing site, where at the end of the line the hotspot stops for a short period before it starts moving in the opposite direction. These movement patterns are illustrated in Fig. 9. For the hotspot we assumed a speed of 1 km/h. Note that these movement patterns are not necessarily realistic, but serve to test the responsiveness and tracking capabilities of the algorithm.

To illustrate that the drone is able to follow the hotspot, Figs. 10–12 plot the distance to the failing site along the x and y-axis for the three movement patterns when $\rho = 8$ for five simulation runs. We expect that the drone follows the hotspot closely as it has a high traffic intensity, meaning that the CSR benefits when the drone serves the users in the hotspot. In these figures, time 0 indicates the moment that the drone is activated

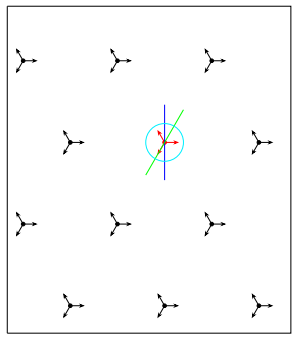

Fig. 9. Illustration of the different movement patterns (cyan, green and blue) of the hotspot, in relation to the failing site and still operational sites.

above the failing site and we see that the drone is able to find and follow the movement of the hotspot. However, we also notice that the drone always slightly lags behind the hotspot, which is because the drone has to follow the hotspot and does in no way predict the path of the hotspot. Furthermore, Figs. 11 and 12 show that the y-coordinate does not follow the hotspot to the point furthest away from the failing site. This can be explained by the fact that even for a hotspot with a high traffic intensity, it may be better to move into the direction of the hotspot, but not right above it, as we have also seen in Fig. 2(b).

Furthermore, we observe in Figs. 10–12 that the drone follows slightly different trajectories for the various simulation runs, which is caused by the different user dynamics in each of the simulation runs. Moreover, as in all simulation runs (of the same scenario) the drone follows a similar trajectory, we conclude that the proposed algorithm is able to adapt to changing environments.

Similarly to the analysis of the convergence time, the presented results are for CM 7, with the other CMs except 2 and 5 (which had bad performance as indicated in Table III) showing similar behavior.

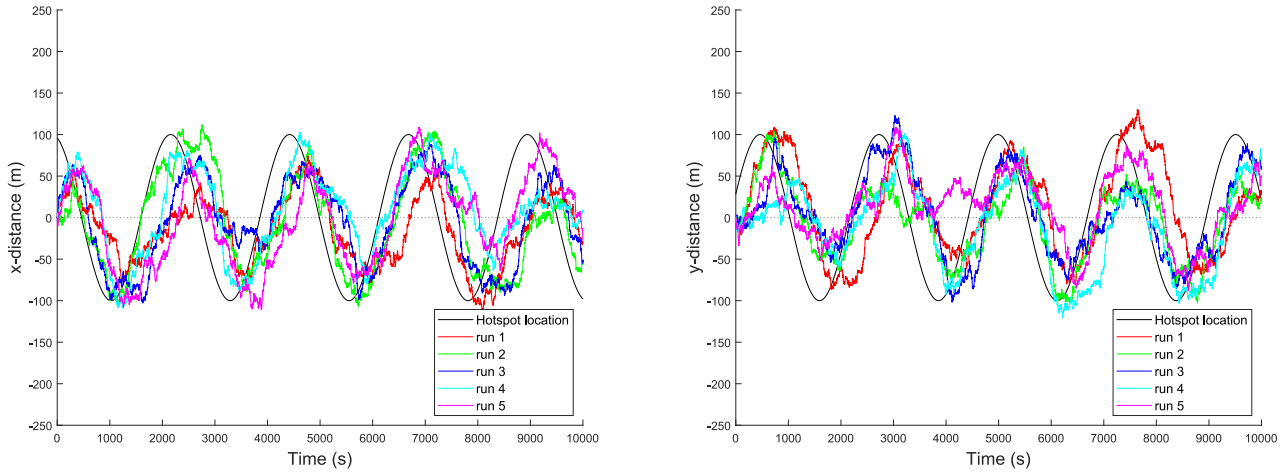

Fig. 10. Circular movement of hotspot (cyan circle in Fig. 9). (a) Distance to failing site along x-axis. (b) Distance to failing site along y-axis.

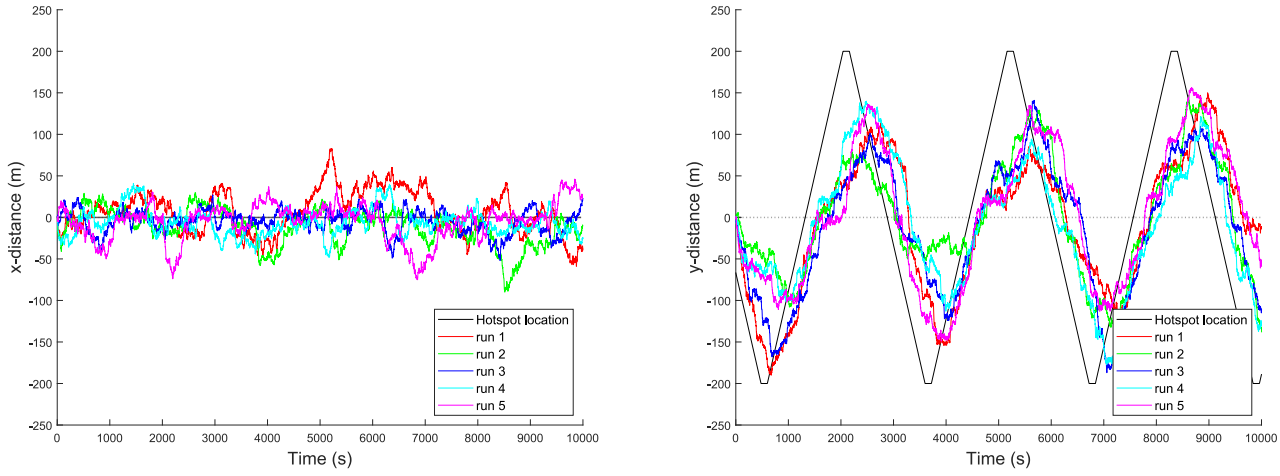

Fig. 11. Line movement of hotspot off azimuth direction (blue line in Fig. 9). (a) Distance to failing site along x-axis. (b) Distance to failing site along y-axis.

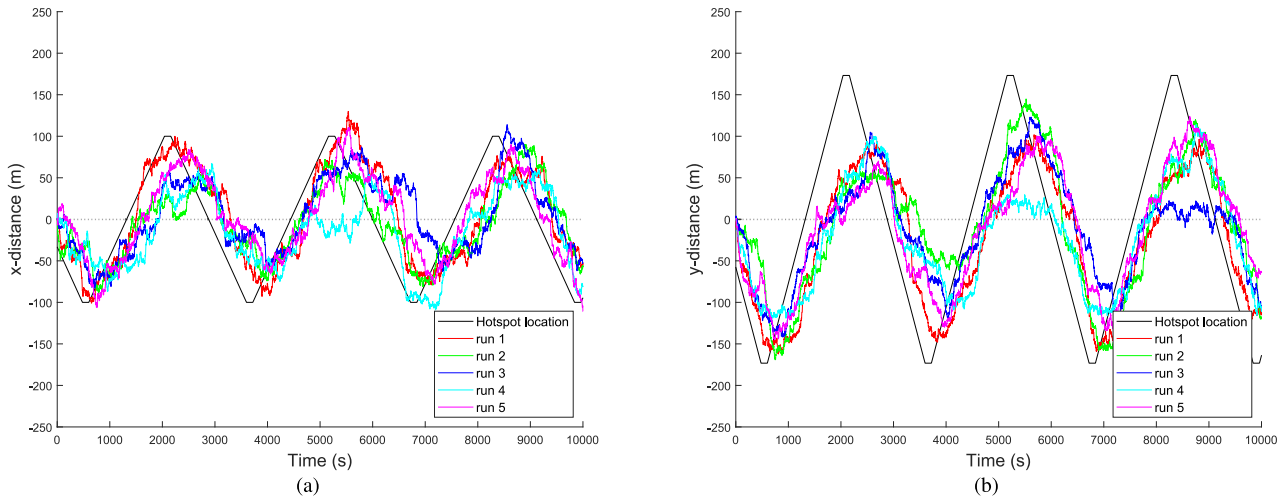

Fig. 12. Line movement of hotspot along azimuth direction (green line in Fig. 9). (a) Distance to failing site along x-axis. (b) Distance to failing site along y-axis.

IX. Conclusion

In this paper we have proposed and evaluated a data-driven algorithm for steering a drone base station in order to optimize the CSR in a scenario with a failing site and emergence of a hotspot. To adjust the drone position, our algorithm leverages real-time measurable data in an online manner, and does not require pre-deployment training or knowledge of the propagation environment, antenna features, location of the hotspot or traffic density.

Our algorithm significantly improves the CSR compared to a setting without a drone, but also when compared to the algorithm of [22] even though our algorithm only adjusts the x and y-coordinates and not the altitude or a cell selection bias as these turned out to have a small impact. Moreover, our algorithm is able to find a near-optimal position within a fairly short amount of time. In addition we demonstrated that our algorithm has the ability to track the optimal position in case of a moving hotspot.

In future research it would be interesting to investigate settings with a broader range of traffic types, where the generic choice of the control metric might prove beneficial. Further topics like deployment algorithms for multiple drones in this scenario or the use of cell outage compensation would be interesting subjects for future research as well.

References

[1] 5G!Drones, EU H2020 project, 2019–2022, www.5gdrones.eu

[2] M. Mozaffari, W. Saad, M. Bennis, Y.-H. Nam, and M. Debbah, "A tutorial on UAVs for wireless networks: Applications, challenges, and open problems," *IEEE Commun. Surv. Tut.*, vol. 21, no. 3, pp. 2334–2360, Thirdquarter 2019.

[3] M. Mozaffari, A. Taleb Zadeh Kasgari, W. Saad, M. Bennis, and M. Debbah, "Beyond 5G with UAVs: Foundations of a 3D wireless cellular network," *IEEE Trans. Wireless Commun.*, vol. 18, no. 1, pp. 357–372, Jan. 2019.

[4] T. Akram, M. Awais, R. Naqvi, A. Ahmed, and M. Naeem, "Multicriteria UAV base stations placement for disaster management," *IEEE Syst. J.*, vol. 14, no. 3, pp. 3475–3482, Sep. 2020.

[5] F. Al-Turjman, J. P. Lemayian, S. Alturjman, and L. Mostarda, "Enhanced deployment strategy for the 5G drone-BS using artificial intelligence," *IEEE Access*, vol. 7, pp. 5999–76008, 2019.

[6] E. Kalantari, H. Yanikomeroglu, and A. Yongacoglu, "On the number and 3D placement of drone base stations in wireless cellular networks," in *Proc. IEEE 84th Veh. Technol. Conf.*, 2016, pp. 1–6.

[7] W. Shi et al., "Multiple drone-cell deployment analyses and optimization in drone assisted radio access networks," *IEEE Access*, vol. 6, pp. 12518–12529, 2018.

[8] F. Pasandideh, T. D. e Silva, A. A. S. da Silva, and E. P. de Freitas, "Topology management for flying ad hoc networks based on particle swarm optimization and software-defined networking," *Wireless Netw.*, vol. 28, pp. 1–16, 2022.

[9] X. Li, "Deployment of drone base stations for cellular communication without apriori user distribution information," in *Proc. IEEE 37th Chin. Control Conf.*, 2018, pp. 7274–7281.

[10] R. Ghanavi, E. Kalantari, M. Sabbaghian, H. Yanikomeroglu, and A. Yongacoglu, "Efficient 3D aerial base station placement considering users mobility by reinforcement learning," in *Proc. IEEE Wireless. Commun. Netw. Conf.*, 2018, pp. 1–6.

[11] R. de Paula Parisotto, P. V. Klaine, J. P. B. Nadas, R. D. Souza, G. Brante, and M. A. Imran, "Drone base station positioning and power allocation using reinforcement learning," in *Proc. IEEE 16th Int. Symp. Wireless Commun. Syst.*, 2019 pp. 213–217.

[12] P. V. Klaine, J. P. B. Nadas, R. D. Souza, and M. A. Imran, "Distributed drone base station positioning for emergency cellular networks using reinforcement learning," *Cogn. Comput.*, vol. 10, pp. 790–804, 2018.

[13] D. Prado, S. Inca, D. Martín-Sacristán, and J. F. Monserrat, "Comparison of optimization methods for aerial base station placement with users mobility," in *Proc. IEEE Eur. Conf. Netw. Commun.*, 2019, pp. 485–489.

[14] H. Ahmadi, K. Katzis, and M. Z. Shakir, "A novel airborneself-organising architecture for 5G networks," in *Proc. IEEE 86th Veh. Technol. Conf.*, 2017, pp. 1–5.

[15] S. Zhang and N. Ansari, "3D drone base station placement and resource allocation with FSO-based backhaul in hotspots," *IEEE Trans. Veh. Technol.*, vol. 69, no. 3, pp. 3322–3329, Mar. 2020.

[16] D. Wu, X. Sun, and N. Ansari, "An FSO-based drone assisted mobile access network for emergency communications," *IEEE Trans. Netw. Sci. Eng.*, vol. 7, no. 3, pp. 1597–1606, Jul.–Sep. 2020.

[17] E. T. Michailidis, N. Nomikos, P. S. Bithas, D. Vouyioukas, and A. G. Kanatas, "Optimal 3-D aerial relay placement for multi-user MIMO communications," *IEEE Trans. Aerosp. Electron. Syst.*, vol. 55, no. 6, pp. 3218–3229, Dec. 2019.

[18] M. A. Kishk, A. Bader, and M.-S. Alouini, "On the 3-D placement of airborne base stations using tethered UAVs," *IEEE Trans. Commun.*, vol. 68, no. 8, pp. 5202–5215, Aug. 2020.

[19] T. R. Pijnappel, J. L. van den Berg, S. C. Borst, and R. Litjens, "Drone-assisted cellular networks: Optimal positioning and load management," in *Proc. IEEE 93rd Veh. Technol. Conf.*, 2021, pp. 1–6.

[20] A. Al-Hourani, S. Kandeepan, and S. Lardner, "Optimal LAP altitude for maximum coverage," *IEEE Wireless Commun. Lett.*, vol. 3, no. 6, pp. 569–572, Dec. 2014.

[21] C. Boucetta, A. Dridi, H. Moungla, H. Afifi, and A. E. Kamal, "Optimizing drone deployment for cellular communication coverage during crowded event," in *Proc. IEEE Mil. Commun. Conf.*, 2019, pp. 622–627.

[22] T. R. Pijnappel, J. L. van den Berg, S. C. Borst, and R. Litjens, "Data-driven optimization of drone-assisted cellular networks," in *Proc. IEEE 17th Int. Conf. Wireless Mobile Comput., Netw. Commun.*, 2021, pp. 233–240.

[23] 3rd Generation Partnership Project, "Study on channel model for frequencies from 0.5 to 100 GHz," 3GPP, Sophia Antipolis, France, Tech. Rep. 38.901 v16.1.0, 2019.

[24] F. Gunnarsson et al., "Downtilted base station antennas - a simulation model proposal and impact on HSPA and LTE performance," in *Proc. IEEE 68th Veh. Technol. Conf.-Fall*, 2008, pp. 1–5.

[25] "Propagation data and prediction methods for the design of terrestrial broadband millimetric radio access systems operating in a frequency range of about 20–50 GHz," Rec. P1410-2, International Telecommunications Union, Geneva, Switzerland, 2003.

[26] R. Fraile, J. F. Monserrat, J. Gozálvez, and N. Cardona, "Mobile radio bi-dimensional large-scale fading modelling with site-to-site cross-correlation," *Eur. Trans. Telecommun.*, vol. 19, pp. 101–106, 2008.

[27] 3rd Generation Partnership Project, "LTE; Evolved universal terrestrial radio access (E-UTRA); radio frequency (RF) system scenario," 3GPP, Sophia Antipolis, France, Tech. Rep. 36.942, v16.0.0, 2020.

[28] The European Commission, Official journal of the European Union, "L152," vol. 62, Jun. 11, 2019. [Online]. Available: https://eur-lex.europa.eu/legal-content/EN/TXT/HTML/?uri=OJ:L:2019:152:FULL

[29] A. Al-Hourani, S. Kandeepan, and A. Jamalipour, "Modeling air-to-ground path loss for low altitude platforms in urban environments," in *Proc. IEEE Glob. Commun. Conf.*, 2014, pp. 2898–2904.

[30] Ericsson, "Ericsson antenna system catalog 2021," 2021, pp. 487–494.